EUROFUSION WPDTT1-PR(16) 15815

N Pelekasis et al.

# Static Arrangement of a Capillary Porous System (CPS): Modelling

Preprint of Paper to be submitted for publication in
Fusion Engineering and Design

This work has been carried out within the framework of the EUROfusion Consortium and has received funding from the Euratom research and training programme 2014-2018 under grant agreement No 633053. The views and opinions expressed herein do not necessarily reflect those of the European Commission.

# Static Arrangement of a Capillary Porous System (CPS): Modelling

**Nikos Pelekasis & Lefteris Benos**

*Dpt. Mech. Eng. University of Thessaly, Volos Greece 38334*

The static arrangement is studied of a thin CPS wafer which is filled from below with a liquid metal. The CPS is modelled as a thin cylindrical disk that is either resting on a flat wall or is embedded in a cylindrical container with long walls. In both cases, it is in contact with a reservoir that provides liquid lithium. Isothermal conditions are considered and a liquid metal layer is assumed to have been established on top of the CPS and reached an axisymmetric static arrangement. A numerical solution is obtained via the finite element methodology that solves the Young-Laplace equation which incorporates surface tension, gravitational, pressure and electrostatic forces. The layer thickness is predicted at static equilibrium as a function of the imposed pressure drop across the wafer, i.e. between the reservoir and the surrounding medium, and the wetting and dielectric properties of the liquid metal. It is seen that at large reservoir overpressure surface tension balances pressure forces and the liquid metal assumes the form of an almost hemispherical drop of small radius. Gravity is not important in this limit. As the pressure drop decreases the drop assumes an oblate shape and a thin film is gradually formed that entirely covers the CPS and extends onto the wetted rigid substrate. In this range, gravity balances pressure drop and surface tension and the film thickness is on the millimeter range, which is relatively large and has negative implications on the stability of the liquid metal layer as the electric field strength increases. Below a certain pressure drop the film becomes very thin, on the order of μm, and the disjoining pressure is seen to balance the imposed pressure drop across it. In this regime a higher external pressure is required in order to overcome the strong repulsive force from the thin liquid metal layer. Such static arrangements are favored in terms of stability of the CPS against $\vec{j} \times \vec{B}$ effects.

Keywords: PFCs, CPS, wetting, pressure drop, disjoining pressure, film thickness, electric stresses, drop ejection

## 1. Introduction

Free surface plasma facing components (PFCs) constitute one of the most critical technological challenges of future fusion reactors since they should have the ability to withstand power densities of the order up to 100 MW/m$^2$ for off-normal events such as edge-localized modes (ELM's) and disruptions. Based on available data from fusion reactors that are in operation, e.g. JET, divertor walls made of tungsten can withstand heat loads up to 20 MW/m$^2$. Beyond this level the plasma-wall interaction that is generated by such events is seen to cause problems such as erosion, thermal stresses, thermal fatigue and plasma contamination which may irreversibly impair the operation of the reactor. In order to circumvent the above problems liquid metals are considered as alternative plasma facing components (PFCS) [1,2,3]. The self-cooling and self-annealing properties of flowing liquids increase their life cycle as they interact with the scrape-off-layer of the fusion reactor. The flow pattern of liquid metals employed for protection of the divertor region and the blanket first wall is characterized by the formation of a free surface that is subjected to the electromagnetic field and heat load generated by the plasma.

PFC's involving free flowing films of liquid metals are susceptible to shear instabilities as a result of the film speed and thickness, on the order of 1 cm, required to exhaust the incoming heat flux [4,5]. Recent experiments at the ISTTOK tokamak [6] and a first principle study [7] validate the deflection mechanism of a liquid metal jet or drop moving inside an electromagnetic field as a result of $\vec{j} \times \vec{B}$ effects. The deflection increased with increasing magnetic field intensity and drops were observed to hit the collector walls.

As an alternative concept, a porous system that acts as a capillary pump pushing liquid metal through a porous medium has been employed [8]. In this concept capillary action is of central importance for renewing the liquid metal, typically lithium, which is in contact with plasma. As an alternative to lithium, liquid tin is envisioned as PFC, due to its low reactivity and much wider liquid state temperature range, which provides much higher extracting power from fusion plasmas [9]. Capillarity and wetting on the porous substrate is expected to stabilize the liquid metal against $\vec{j} \times \vec{B}$ effects and drop ejection [11], and this is a key issue underpinning the reliability of liquid metals as PFC's. Nevertheless, drop ejection and splashing has been reported during operation of CPS systems in the literature [11,18], especially when $\vec{j} \times \vec{B}$ forces are present.

In the present study, the static arrangement of a CPS system is investigated in order to assess the thickness of the liquid metal film that rests on top of it protecting it

*Corresponding author's email: pel@uth.gr*

from surrounding plasma. Fig. 1a shows the CPS system employed at ENEA Frascati. Owing to its complex curved geometry, a simplified static arrangement is investigated, fig. 1b, which provides a simplified schematic diagram, that resembles the wicking process envisioned for NSTX [12]. In the absence of reliable experimental measurements of the static film thickness we examine the simplified arrangement depicted in figs. 2a,b,c where filling from below is envisioned, with the pressure drop between the liquid metal reservoir and the surrounding medium treated as a parameter that determines the film thickness, given the liquid metal properties and the topography of the CPS system.

In section 2 the problem formulation is presented along with the major simplifying assumptions for the case of an axisymmetric porous wafer. The effect of an external electric field is included as a means to address the impact of field forces on the static arrangement. In section 3 the numerical methodology is presented via the finite element method that is most suitable for free surface problems. Next, in Section 4.1 a parametric study is presented highlighting the relative importance of capillarity, gravity and pressure drop as the reservoir overpressure decreases. In section 4.2 the importance of electric stresses is shown in the static arrangement and the ensuing dynamic stability of the liquid metal layer [13]. Finally, in Section 5 the importance of the disjoining pressure is stressed [14] in maintaining a very thin film of liquid metal coating on top of the porous structure for negligible reservoir overpressures -filling of the porous structure will be performed under vacuum conditions [12]- conclusions are drawn and directions for future research are proposed.

## 2. Problem Formulation

We are interested in the static arrangement of a CPS system as a function of the overpressure, $\Delta P=P_r-P_{out}$, between the reservoir and the surrounding medium and the physical properties of the employed liquid metal. Fig. 2 illustrates the anticipated static configuration as $\Delta P$ decreases, to be verified in the results and discussion section 4. We consider a porous system shaped as a circular disk of small thickness, on the order of 1 mm.

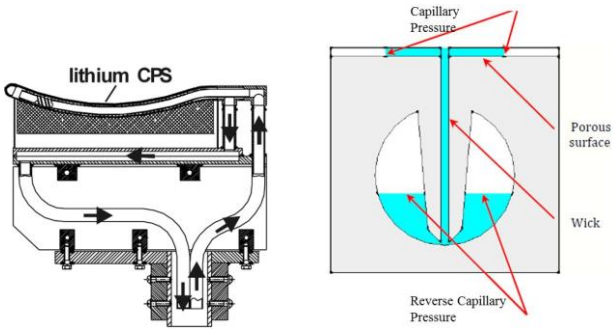


(a) (b)

**Fig. 1.** Schematic diagram of the CPS arrangement in (a) ENEA Frascati [8] and (b) NSTX-U [12].

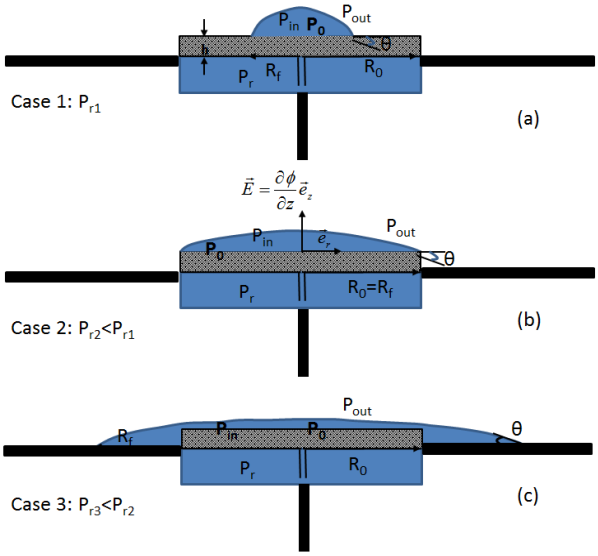


**Fig. 2.** Schematic of the geometry studied in the present study and the resulting static configurations.

The characteristic pore diameter is on the order of tenths of μm's in which case a static arrangement cannot be obtained with the liquid metal partially filling the porous wafer. The porous system is in contact with a reservoir that provides the liquid metal via a thin wick. Static arrangements are obtained with partial or full coverage of the porous structure, depending on the reservoir overpressure ΔP, figs. 2a,b,c, for fixed radius $R_0$ of the porous wafer. We are primarily interested in predicting the thickness of the film that is formed on top of the porous structure at static equilibrium as well as the extent of its coverage. Since it is anticipated that, for low enough overpressures, the radius of the porous wafer is not enough to secure a static arrangement the liquid metal is allowed to cover part of a solid substrate that extends beyond the porous structure. This is done in an effort to account for the protection area envisioned on the sides of CPS structures in order to recover liquid metal that spills out of the porous layer [12]. Once the static arrangement is achieved, the pore size in the CPS does not affect the shape of the liquid metal layer that may entirely cover it. The stability of the obtained static configuration during the dynamic evolution of the liquid metal layer is not examined herein nor the time interval required for static equilibrium to be achieved.

In order to assess the impact of field forces on the liquid metal layer that covers the porous system, the effect of an external electric field $\vec{E}=\frac{\partial\phi}{\partial z}\vec{e}_z=a\vec{e}_z$ is also considered that is aligned with the axis of symmetry of the porous wafer, fig. 2b. $\phi$ denotes the electric potential while $a$ stands for the partial derivative of $\phi$ with respect to z. The evolution of the shape of the interface is of interest as the intensity of the electric field is increased, aiming at identifying conditions for which electric stresses overwhelm adhesion forces and conical angle formation is obtained [15]. The liquid metal is treated as a very electrically conducting material in comparison with the external medium. Such an arrangement is known to be subject to instability and jet formation leading to drop ejection [13] for a strong

enough electric field. The dynamic evolution of the liquid metal layer covering the porous structure is not examined in the present study and is left for a future investigation.

The normal force balance on the interface between the liquid metal layer and the surrounding medium holds at equilibrium:

$$\vec{\mathrm{r}} = \vec{\mathrm{r}}_{\mathrm{s}}(\mathrm{r},\mathrm{z}): \quad \vec{\mathrm{n}} \cdot \left[ \left( \mathrm{P}_{\mathrm{in}} - \mathrm{P}_{\mathrm{out}} \right) \underline{\underline{\mathrm{I}}} + \left( \underline{\underline{\tau}}_{\mathrm{el}}^{\mathrm{out}} - \underline{\underline{\tau}}_{\mathrm{el}}^{\mathrm{in}} \right) \right] + 2\sigma H \vec{\mathrm{n}} = 0 \quad (1)$$

in cylindrical coordinates: $\vec{n} = \left( \vec{e}_z - z_r \vec{e}_r \right) / \sqrt{1+z_r^2}$ (2)

where $\vec{r}_s, \vec{n},$ denote the position and normal vectors of the interface, respectively, σ interfacial tension, H the mean curvature, $\underline{\underline{\mathrm{I}}}$ the unit tensor and $\underline{\underline{\tau}}_{el}$ electric stresses at the interface.

$$P_{in} = P_r - \rho g h - \rho g z_0, \quad P_0 = P_r - \rho g h, \qquad (3a,b)$$

denote the pressure of the liquid metal layer at the interface with the surrounding medium and the porous wafer, respectively, h the thickness of the porous wafer, $z_0$ the film thickness at the axis of symmetry, r=0, ρ the liquid metal density and g the acceleration due to gravity.

The liquid metal layer is treated as a conducting drop in which case the electric potential $\phi$ is constant inside it while $\in \equiv \in_{out} / \in_{in} << 1$, with $\in_{in}, \in_{out}$, denoting the electric permittivity of the liquid metal and surrounding medium, respectively. Furthermore, in this limit the electric stresses at the interface assume the simplified form [13,15]

$$\vec{n}\underline{\underline{\tau}}_{el} = \vec{n} \cdot \left( \underline{\underline{\tau}}_{el}^{out} - \underline{\underline{\tau}}_{el}^{in} \right) = \vec{n} \frac{\varepsilon_{out}}{2} \left( \frac{\partial \Phi}{\partial n} \right)^2 \approx \vec{n} \frac{\varepsilon_{out}}{2} \frac{a^2}{1+z_r^2}; \quad (4)$$

in the calculations to be presented in the following we have set $\in_{out} = 1, \in_{out} = 40,$ for completeness. In obtaining the above formula we assume that the film is thin in which case $\frac{\partial \phi}{\partial n} \approx \frac{\partial \phi}{\partial z} = a$. This assumption gradually loses validity as the film deforms in response to an increasing electric field, however it is a useful first approximation that allows us to avoid a boundary element type approach for a more accurate calculation of the electric potential in the surrounding medium [13,16].

The problem formulation is complemented by imposition of the conditions pertaining to the unknown shape of the interface z=z(r) for cylindrical coordinates:

$$r = 0: \quad \frac{dz}{dr} \equiv z_r = 0 \text{ due to axisymmetry} \qquad (5a)$$

$$r = R_f: z = 0, \quad \vec{t} \cdot \vec{e}_z = \frac{z_r}{\sqrt{1+z_r^2}} = -\sin\theta \qquad (5b)$$

where $\vec{t}$ is the tangential unit vector of the interface. The last condition sets the contact angle at the three phase contact line, circle in the present case due to axisymmetry, where the liquid metal layer is in contact with the solid substrate and the surrounding medium. Partial wetting is assumed between the liquid metal and the substrate in the sense that [17]

$$\mathrm{S} \equiv \sigma_{\mathrm{SV}} - (\sigma_{\mathrm{SL}} + \sigma_{\mathrm{LV}}) < 0 \qquad (6a)$$

so that definition of a contact angle via the static balance

$$\sigma_{\mathrm{SV}} - \sigma_{\mathrm{SL}} = \cos\theta \sigma_{\mathrm{LV}} \rightarrow S = \sigma_{\mathrm{LV}} \left( -1 + \cos\theta \right) < 0 \qquad (6b)$$

There are three interfaces across which an energy (per unit of contact area) exists. These energies per area are denoted by $\sigma_{SV}$ for the bare solid-vapor interface, $\sigma_{SL}$ for the liquid-solid interface, and $\sigma_{LV} = \sigma$ for the liquid-vapor interface.

Eqs (1) and (5a,b) constitute the problem formulation in the absence of an external electric field, in which case the z coordinate of the interface as a function of the radial distance, z(r), along with the radial position of the contact point, $R_f$, are the unknowns of the problem. Once the static arrangement is obtained then the mass of the liquid metal that is pinned onto the substrate is calculated

$$M = 2\pi\rho \int_0^{R_f} z(r) r dr \qquad (7)$$

and the effect of the electric field on the static configuration is captured by setting the contact point at $r=R_f$ while leaving the contact angle as an unknown, see also [13]. The latter is calculated in the post-processing phase of the numerical solution via eq. 5b. In both cases the pressure at the interface between the porous structure and the liquid metal layer, $P_0$ is fixed, eq. 3b.

Reformulating the problem in dimensionless variables using the radial position of the contact point, $R_f$, as the characteristic length scale, the following dimensionless variables arise:

$$Bo \equiv \frac{\rho g R_f^2}{\sigma}, \; Bo_{El} \equiv \frac{R_f a^2}{\sigma}, \; \Delta P \equiv \frac{P_0 - P_{out}}{\sigma / R_f}, \qquad (8)$$

measuring the relative importance between gravity, electric stresses, pressure drop and surface tension. The three phase contact angle and electric permittivity ratio, $\theta, \in_{in} / \in_{out}$, complete the list of the dimensionless variables that govern the static response of the system under examination. When the radial position, $R_f$, is set the dimensionless pressure drop is part of the problem solution. When the pressure drop, $P_0$-$P_{out}$, is set a preliminary length scale, $\hat{R} = \sigma / (P_0 - P_{out})$, is obtained by setting $\Delta P = 1$. The radial position at the contact point is then calculated in dimensionless form, $R_f / \hat{R}$, as part of the numerical solution.

## 3. Numerical Methodology

The normal force balance described in eq. (1) is discretized using the finite element methodology, with the unknown z coordinate of the liquid metal layer

interface with the surrounding medium described via a number of quadratic Lagrangian basis functions $B_i(r)$ :

$$z(r)=\sum_{i=1}^{N} z_i B_i(r) \tag{9}$$

where $z_i$ denotes the axial position of the N interfacial nodes. We resort to the weak formulation of eq. (1) by introducing the following identity from differential geometry that reduces the order of differentiation in the curvature:

$$\vec{n}2H=\frac{\partial \vec{t}}{\partial s}-\frac{\vec{n}}{R_2}, \quad \frac{1}{R_2}=-\frac{z_r}{r\sqrt{1+z_r^2}}, \tag{10}$$

where $R_2$ denotes the second curvature of the interface; subscript r denotes differentiation and $ds=\sqrt{1+z_r^2}\,dr$ the differential length in the azimuthal direction of the interface. Thus, only the z component of the normal force balance survives in the weak formulation since the r component integrates out due to axisymmetry:

$$\int_0^{R_f} B_i r\left(P_0-P_{out}\right)dr-\sigma r\sin\theta\Big|^{r=R_f}-\int_0^{R_f}\frac{\sigma r z_r}{\sqrt{1+z_r^2}}\frac{dB_i}{dr}dr-$$
$$-\rho g\int_0^{R_f} B_i r z dr+\frac{a^2\in_{out}}{2}(1-\in)\int_0^{R_f}\frac{rB_i}{1+z_r^2}dr=0, \tag{11}$$

Eq. (10) along with eq. (5b) are solved for the axial position of the liquid metal layer z(r) and the radial position, $R_f$, of its contact point on the substrate, for given overpressure, $P_0$-$P_{out}$. Upon application of eq. (10) on each one of the N nodal points of the finite element mesh and addition of the individual components we obtain an integral force balance on the liquid metal "drop" resting on the substrate:

$$\int_0^{R_f} r\left(P_0-P_{out}\right)dr-\sigma r\sin\theta\Big|^{r=R_f}-\rho g\int_0^{R_f} r z dr+$$
$$\frac{a^2\in_{out}}{2}(1-\in)\int_0^{R_f}\frac{r}{1+z_r^2}dr=0, \tag{12}$$

The latter integral force balance can be used in order to examine the relative importance of the different factors that determine the static equilibrium.

The resulting set of nonlinear algebraic equations is solved in an iterative fashion via the Newton-Raphson method until convergence. Each iteration involves inversion of a banded matrix. As the overpressure decreases the shape becomes flat while vanishing at the equator, see relevant discussion in the next section, and iterations fail to converge below a certain threshold value.

As an alternative approach, the pressure at the film porous layer interface, $P_0$, is treated as an unknown while fixing the radial position of the contact point $R_f$. In the present study, it was seen that the Newton-Raphson procedure converged much faster in this fashion thus affording an extension of the parametric study to quite small, even negative, overpressures.

Once the static arrangement is obtained for fixed overpressure, the mass of liquid metal contained within the interface with the surrounding medium is calculated via eq. (7) and the static arrangement is recalculated by gradually increasing the intensity of the electric field a. In this case the contact angle is not fixed. Rather, the radial position $R_f$ at the contact point is set to the value obtained at static equilibrium before the activation of the electric field [13]. The pressure $P_0$ is treated as an unknown since this study serves as a first attempt to capture the effect of external electromagnetic field forces on the liquid metal layer and, possibly, obtain plausible conjectures regarding its stability once plasma activity is turned on [18].

As a benchmark study we calculate the shape of a polymeric drop that rests on a solid substrate with material properties pertaining to the study in reference [13]:

$$Bo=\frac{\rho g R_f^2}{\sigma}\approx 0.33,\ \theta=60^o,\ \frac{\in_{in}}{\in_{out}}\approx 40,\ Bo_{El}\equiv\frac{R_f a^2}{\sigma}; \tag{13}$$

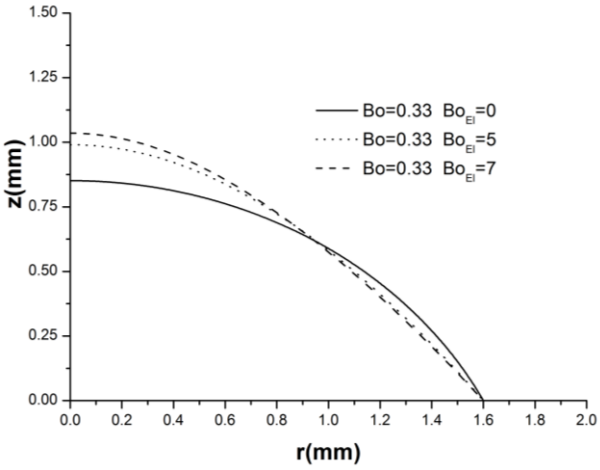


**Fig. 3.** Shape evolution with increasing electric field intensity; 200 quadratic Lagrangian elements were used in the calculations.

As can be deduced upon comparing fig. 3 with fig. 6a from [13], the static solutions in the absence of an external electric field are in complete agreement, while the static shape that is subject to electric stresses appears to be flatter at the pole in fig. 3. This is a result of the simplifying assumption employed in the present study in the calculation of electric stresses, eq. (4), that assumes an almost flat shape thus underestimating the impact of electric stresses as the field strength increases. However, the tendency for the pole region to gradually exhibit a stronger axial displacement and a larger curvature is clearly illustrated and its impact on the stability of the liquid metal layer will be discussed in the next section.

## 4. Results and Discussion

The above methodology was implemented in order to perform a parametric study on the effect of external overpressure on the shape and thickness of the liquid

metal layer that coats the porous layer at static equilibrium. Liquid lithium was used as the operating fluid. The geometric configuration envisioned is the one depicted in fig. 2 pertaining to a porous disk of 10 cm radius and 1 mm thickness. Small overpressures, $P_0$-$P_{out}$, are considered since the imbibition process of the liquid layer as well as its operation will be at near vacuum conditions [10,11,12], with the liquid metal filling the porous matrix from below. The reservoir pressure is $\rho g h_0 \approx 5$ Pa above $P_0$ based on the thickness of the porous layer. The approach via setting the radial position of the contact line is adopted in order to optimize convergence of the iterative procedure, with a finite element mesh ranging between 500 and 4000 quadratic elements in order to capture abrupt changes in the curvature of the interface. For lithium, a characteristic Bond number based on the radial position at contact, $R_f$, is Bo≈150 whereas the contact angle θ is set to 30° [19].

Three regimes are identified of the static arrangement assumed by the liquid metal layer. In the first one the liquid metal forms a drop that rests on top of the porous layer covering part of it, in the manner illustrated in fig. 2a. Fig. 4a depicts the evolution of the interfacial shape as the radial position of the contact line increases up to the point where it completely covers the porous layer whose radius is 10 cm. The two axes are drawn in scale so that the gradual formation of a thin film becomes evident as the reservoir overpressure decreases.

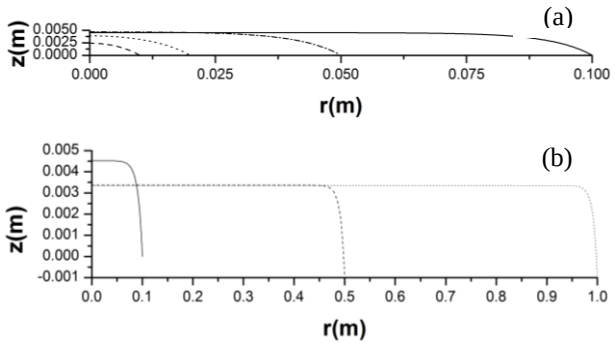


**Fig. 4.** Evolution of the shape of the interface between the liquid metal layer and the surrounding medium with decreasing reservoir overpressure; (a) dashed line: $P_r$-$P_{out}$=49 Pa, dotted line: $P_r$-$P_{out}$=35 Pa, dash-dot line: $P_r$-$P_{out}$=31 Pa, solid line: 29 Pa; (b) solid line: 29 Pa, dashed line: $P_r$-$P_{out}$=23 Pa, dotted line: $P_r$-$P_{out}$=22.9 Pa (axes in fig 4b are not drawn in scale).

As can be gleaned from fig. 4a, with increasing overpressure the dominant balance is formed by pressure and surface tension and the shape of the liquid metal layer approaches that of a hemishere. In fact if the pressure drop between the reservoir and the interface with the porous layer, $P_r$-$P_0$, is subtracted then the radial position of the contact line $R_f$ roughly scales with the inverse of $\Delta P = P_0 - P_{out}$ reflecting the effect of surface tension, $\Delta P\, \pi R_f^2 \approx \sigma 2\pi R_f$ as gravity becomes subdominant. In this limit the volume of liquid metal that rests on the porous layer, while the latter remains fully covered, decreases. As the overpressure starts decreasing gravity is needed to establish the dominant force balance and the liquid metal layer extends to cover a wider part of the porous layer. The radial position at the contact line increases and the volume of the liquid metal that rests on the porous matrix increases as well until its entire surface is covered by liquid metal. The process shown in fig. 4a is schematically illustrated in figs. 2a,b. In these graphs the porous layer is assumed to be saturated with liquid metal before the liquid metal "drop" spreads to reach static equilibrium. This assumption is corroborated by previous studies accounting for the spreading dynamics of a liquid drop on a saturated porous substrate [20] where the spreading process is shown to take place in a fashion similar to spreading on a dry solid. Furthermore, for a thin enough porous substrate, the saturation process of the substrate takes place much faster than drop spreading, owing to the much larger capillary pressure inside a partly filled porous matrix in comparison with the drop; $\sigma / R_p >> \sigma / R_f$ . Therefore we can safely assume that static equilibrium will be achieved over a saturated substrate. We should also stress that the dynamics and the time scale over which such a state will be reached was not addresed in the present study. However, this may be of central importance in a practical application and will be addressed in a future study.

As the overpressure $P_o$-$P_{out}$ is further decreased the liquid metal spreads over the top of the porous layer and covers part of the solid substrate that is attached to it, see fig. 2c. The volume of liquid metal that covers the porous layer and part of the solid substrate increases significantly as illustrated in fig. 4b. Axes are drawn out of scale due to the very large dimension of the radial direction in comparison with the axial one. The axial location of the interface assumes negative values in the region that extends below the top surface of the porous layer on the solid substrate. Hence the jump in the pressure drop as the liquid metal layer goes beyond the porous matrix in fig. 4b. It should be also pointed out that in this regime the porous layer is entirely embedded within the liquid metal "drop" which spreads out to cover part of the solid substrate that extends beyond the porous matrix, fig. 2. In this regime pressure forces and gravity form the dominant balance. The latter essentially acts to reduce curvature from the top surface, where it is close to zero, to its valus at the contact line. Thus, a very thin boundary layer is generated near the contact point and a very large number of elements is required, on the order of 4000, in order to capture this transition. At the same time, a very thin film forms that extends over a large portion of the solid substrate. Its thickness, $z_{(r=0)}+h_0$, decreases albeit very slowly in comparison with the radial dimension. The latter increases very fast as the pressure drop decreases in order to facilitate the force balance.

### 4.1 Interaction with an External Electric Field

Despite the fact that it generates a thin film the above static arrangement may be subject to instabilities and drop ejection in the presence of electromagnetic forces, the mechanism of which strongly depends on the size of the original layer and its adhesion properties.

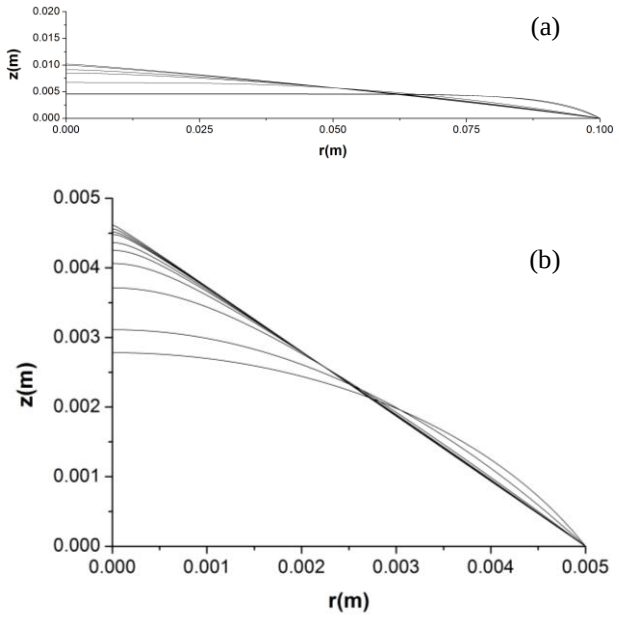


**Fig. 5.** Evolution of the shape of the interface with the porous layer fully covered, with increasing electric field intensity, $\in_{in} / \in_{out} \approx 40$ ; (a) Bo=134, θ=30$^o$ and $Bo_{El}$=0, 25, 625, 1225, 1600, 2500 and 3025; (b) Bo=0.33, θ=60$^o$ and $Bo_{El}$=0, 5, 20, 45, 80, 125, 245, 320 and 500.

Using the static equilibrium obtained in fig. 4a with the top of the porous matrix fully covered, i.e. $R_f$=0.1 m, and gradually increasing the electric field intensity while keeping the mass of the liquid metal within the layer constant, we obtain the sequence of shapes shown in fig. 5a. As a result of the electric stresses the pole section of the layer is elongated in the field direction while the contact angle at the equator decreases in order to maintain the same amount of liquid lithium. The liquid layer thickness increases away from the contact line and its curvature increases as well. Eventually, a conical angle tends to form at the pole with half angle $\theta_c$~75$^o$ and a solution could not be obtained for stronger electric fields. In this limit, given the large value of Bo, gravity is balanced by electric stresses and this determines the size of the conical angle at the pole.

Despite the simplified model employed here for the prediction of electric potential in the surrounding medium, this is a valid description of the static equilibrium. In fact, as the initial size of the lithium layer decreases, e.g. when $R_f$=5 mm, Bo=0.33 and the shape is almost hemispherical, then upon increasing the electric field the electric stresses generate static shapes similar to those observed in [13], see also fig. 3, until the interface of the layer tends to exhibit a conical angle at the pole. It should be stressed that in this regime gravity does not play an important role and the balance between surface tension and electric stress dominates. In addition, it was assumed that the static contact angle is θ=60$^o$ and is larger than the one in fig. 5a, perhaps as a result of erosion. Beyond a certain range of electric field intensities, $Bo_{El}$>500, the solution does not change significantly except for the pole region where the conical angle is formed of θc~47$^o$, fig 5b. The above angle is very close to the angle of 49$^o$ predicted by Taylor [15] for conductive cylinders elongated by the action of electric stresses. Indeed this is verified by more recent studies in the literature [13] where the dynamics of this process is also studied. It was thus predicted that the contact angle that is formed dynamically is smaller than the Taylor angle. Moreover, it was seen [13] that depending on the static contact angle and the field intensity, along with the appearance of the dynamic conical angle, jetting is initiated at the pole region. This process is known to generate small droplets once the jet speed reaches a certain threshold. In that same study it was observed that, depending on the static contact angle and the extent of wetting, dislocation of the entire layer may take place instead of jetting.

The above phenomena provide a plausible mechanism for drop ejection during operation of the CPS subject to electromagnetic forces. It is, of course, understood that during plasma operation the field force will not arise due to the electric field intensity in the divertor region. Rather, it will be a manifestation of $\vec{j} \times \vec{B}$ effects in that same region, which are conjectured to operate in a similar manner leading to similar jetting and drop ejection phenomena. Another important aspect of this study pertains to size effect. In particular, as the size of the layer increases the intensity of the electric field required for the formation of the conical angle decreases, as suggested by $Bo_{El}=R_f\ a^2/\sigma$, since the critical $Bo_{El}$ for conical angle formation is fixed for fixed static contact angle and electric permittivity ratio. Upon comparing the benchmark case, fig. 3, with that in fig. 5b, it is seen that the behavior is very similar at similar Bond numbers. This places a limit in the thickness of the liquid metal layer that protects the porous matrix, if unwanted instabilities are to be avoided. This, however, is not the topic of the present study and is left for a future examination of the dynamic response of the liquid metal layer.

### 4.2 Film Thickness at very small overpressures

The analysis presented in the beginning of this section predicts a thicnesses for the liquid metal layer covering the porous matrix on the order of millimeters for overpressures $P_r$-$P_{out}$ as low as 20 Pa, fig. 4a,b. As thin as they may be such films are susceptible to instabilities in the presence of electromagnetic field forces, see the discussion in section 4.1, that are present during plasma operation. Furthermore, based on the literature the porous matrix is normally filled at near vacuum conditions [12]. In addition, porous matrices saturated with lithium [8,12,21] or tin [9] were seen to be covered by a layer of liquid metal with thickness on the order of several μm's. Consequently, there is need to investigate the thickness of the liquid metal layer that covers the porous matrix at even smaller overpressures, in an effort to achieve much smaller thicknesses that enhance the stability of the protective film. In order to investigate this possibility, the parametric study presented above has to be extended to account for the repulsive force exerted at the interface as a result of its interaction with the solid substrate at very small distances, i.e. micron or submicron level. Such a force will enter the normal force

balance in the form of a disjoining pressure Π that arises by differentiating a long range attractive short range repulsive potential [14] W with respect to the local distance z between the liquid metal interface and the substrate:

$$W = W_0\left[\left(\frac{\delta}{z}\right)^a - \frac{a}{b}\left(\frac{\delta}{z}\right)^b\right], \quad a > b > 1 \qquad (14a)$$

$$\Pi = -\frac{dW}{dz} = W_0\frac{a}{z}\left[\left(\frac{\delta}{z}\right)^a - \left(\frac{\delta}{z}\right)^b\right]. \qquad (14b)$$

Eq. (14) provides a standard form of such an interaction potential [14] with $W_0$ signifying a typical energetic advantage per unit volume as the distance from the solid substrate decreases and δ a characteristic length scale for which the energy is minimized and the interaction force vanishes. Constants a, b, are selected so that the disjoining pressure Π is positive at distances z<δ, indicating repulsion, and negative at distances z from the substrate that are larger than the characteristic scale δ, indicating attraction; a=4 and b=2 are typical selections that can be modified based on the nature of the interacting materials. The interaction potential W is not affected by displacements parallel to the substrate and becomes negligibly small at distances that are significntly larger than δ.

In the absence of an external field force the normal force balance (eq. 1) reads:

$$\vec{r} = \vec{r}_s(r,z): \quad \vec{n}\cdot\left[\left(P_{in} + \Pi - P_{out}\right)\underline{\underline{I}}\right] + 2\sigma H\vec{n} = 0 \qquad (16)$$

The disjoining pressure Π that was added expresses the repulsive force that has to be overcome by the external pressure $P_{out}$ in order to generate films whose thickness is lower than δ.

As was shown in the calculations for the static equilibrium, the distance over which the liquid metal layer extends increases very rapidly with decreasing overpressure while the film thickness decreases at a very slow rate, see Figs. 4a,b, and remains on the millimeter scale. When much thinner films are obtained the disjoining pressure muct be accounted for. For example, and based on the available experimental observations, if the length scale δ for the interaction between lithium and the porous matrix is on the order of 10 μm's then the static arrangement that is anticipated is depicted below, fig. 6. It consists of a thin film with thickness on the order of μm's that covers the porous matrix and that extends over to the neighbouring solid substrate. Since the disjoining pressure becomes infinite exactly at the substrate we envision a static equilibrium that consists of a precursor film of neutral thickness δ=10 μm covering the solid substrate. The overpressure in this case wil be $P_r - P_{out} = \rho g\delta \approx 0.05Pa$ which conforms with the near vacuum conditions under which filling of the porous matrix takes place. In the region at the top of the porous matrix the pressure $P_0$ is below the reservoir pressure by $\rho g h_0$. Therefore, at static equilibrium, the thickness $\delta_f$ of the film that protects the porous matrix will be lower than the characteristic length δ, i.e. a few micrometers, so that a repulsive disjoining pressure Π develops in order to match the pressure difference $P_{out} - P_{in} = P_{out} - \left[P_r - \rho g\left(h_0 + \delta_f\right)\right] = \rho g h_0$.

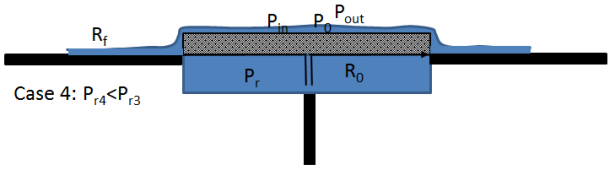


**Fig. 6.** Schematic diagram of the anticipated static arrangement with a film thickness on the order δ~ μm's

Films that are thicker than the characteristic length δ will be obtained at larger pressure drops since the disjoining pressure Π will acquire negative values indicating attraction to the substrate. In this fashion the gap in the parametric study regarding the static arrangement at smaller overpressures than those reported in Figs 4a,b, is filled with more realistic thin films. If the overpressure drops further more, reflecting the repulsive disjoining pressure Π at the interface, then even thinner films can be generated. This qualitative picture will be validated quantitatively in a future numerical investigation.

## 5. Conclusions

The static arrangement of a liquid metal layer that coats a porous matrix was modelled and investigated numerically. It was seen that reducing the overpressure between the reservoir and the surrounding medium thinner films can be obtained. In order to recover the very thin films, thickness on the order of micrometers, reported in the literature, the disjoining pressure must be incorporated in the model. This is expected to bridge the gap in the parametric study regarding the size of the liquid metal layer as the overpressure between the liquid metal reservoir and the external medium decreases. It should be stressed that the porous matrix is assumed to be saturated at all times in which case the pore size does not affect the static arrangement that is obtained.

The static film thickness is an important parameter that will affect the reliability of the CPS during plasma operation. A preliminary numerical study was conducted pertaining to the impact effected on the static arrangement of the liquid metal by the electric stresses that arise upon application of an external electric field. It was thus seen that conical angles may appear as the electric field strength increases. Dynamic operation of the CPS may alter the magnitude of the angle or the time of its appearance. However, based on the relevant literature, for cases of good partial wetting dynamic conical angle formation is followed by jetting and possibly drop ejection. The electric field strength required for such an instability to arise increases with decreasing thickness of the liquid metal layer. Consequently, it is of central importance regarding the feasibility of capillary porous systems in power exhaust

of fusion reactors, to ascertain the actual static arrangement of the structure and perform dynamic studies where the more relevant $\vec{j} \times \vec{B}$ effects are incorporated in the analysis.

## Acknowledgements

This work has been carried out within the framework of the EUROfusion Consortium and has received funding from the Euratom research and training programme 2014-2018 under grant agreement No 633053. The views and opinions expressed herein do not necessarily reflect those of the European Commission.

### References

[1] N.C. Christofilos, Design for a high power-density Astron reactor, Fusion Energy 8 (1989) 97.

[2] F. L Tabarés, Present status of liquid metal research for a fusion reactor, Plasma Phys. Control. Fusion 58 (2015) 014014 (8pp).

[3] Y. Hirooka, G. Mazzitelli, S. Mirnov, M. Ono, M. Shimada and F. L. Tabares, A Review of the Present Status and Future Prospects of the Application of Liquid Metals for Plasma-Facing Components in Magnetic Fusion Devices, Fusion Sci. Technol. 68 (2015) 477-483.

[4] A.Y. Ying, N. Morley, S. Smolentsev, K. Gulec, P. Fogarty, Free surface heat transfer and innovative designs for thin and thick liquid walls, Fusion Eng. Des. 49–50 (2000) 397–406.

[5] K. Itoh, M. Nakamura, H. Kumamaru & Y. Kukita, Internal-Shear Mode Instabilities on High-Speed Liquid Jet (II) Experimental Analysis of Curved Target Flow, Nuclear Sci. Technol. 41 (2004) 809–816.

[6] R.B. Gomes, C. Silva, H. Fernandes, P. Duarte, I. Nedzelskiy, O. Lielausis, et al., ISTTOK tokamak plasmas influence on a liquid gallium jet dynamic behavior, Nucl. Mater. 415 (2011) S989–S992.

[7] N.A. Pelekasis, L.Th. Benos, and R.B. Gomes, Deflection of a liquid metal jet/drop in a tokamak environment, Fusion Eng. Des 89 (2014) 2930-2936.

[8] A.V. Vertkov, I.E. Lyublinski, M.Yu. Zharkov, V.V. Semenov, E.A. Azizov, V.B. Lazarev, S.V. Mirnov, Progress in development and application of lithium based components for Tokamak, Fusion Eng. Des 89 (2014) 996-1002.

[9] T.W. Morgan, D.C.M. van den Bekerom, G. De Temmerman, Interaction of a tin-based capillary porous structure with ITER/DEMO relevant plasma conditions, Nucl. Mater. 463 (2015) 1256–1259.

[10] G. Mazitelli, M.L. Apicella, M. Marinucci, C. Mazzotta, V. Pericoli Ridolfini, O.Tudisco, et al., Lithium as a liquid limiter in FTU, IN: 21ST IAEA Fusion Energy Conference, Chengdu, China, 2006, EX/P4–16.

[11] V. Philipps, Comments on the assessment of liquid metal solutions for DEMO (WPDTT1 Meeting LM-2), Frascati Nov. 2015.

[12] P. Rindt, Conceptual design of pre-loaded liquid lithium divertor targets for NSTX-U (Master Thesis), Univ. Eindhoven, Netherlands, 2015.

[13] S. N. Reznik, A. L. Yarin, A. Theron and E. Zussman, Transient and steady shapes of droplets attached to a surface in a strong electric field, Fluid Mech. 516 (2004) 349–377.

[14] J.N. Israelachvili, Intermolecular and surface forces, 3rd Edition: Amsterdam, 2011.

[15] G. I. Taylor, The force exerted by an electric field on a long cylindrical conductor. Proc. R. Soc. Lond. A 291 (1966) 145–158.

[16] Miksis, M., Shape of a drop in an electric field, Phys. Fluids, 24 (11) (1981) 1967–1972.

[17] S. Middleman, Modeling Axisymmetric Flows: Dynamics of films jets and drops, Academic Press Inc. San Diego California, 1995.

[18] M.A. Jaworski, S.P. Gerhardt, N.B. Morley, T. Abrams, R. Kaita, J. Kallman et al., Macroscopic motion of liquid metal plasma facing components in a diverted plasma, Nucl. Mater. 415 (2011) S985–S988.

[19] P. Fiflis, A. Press, W. Xu, D. Andruczyk, D. Curreli, D.N. Ruzic, Wetting properties of liquid lithium on select fusion relevant surfaces, Fusion Eng. Des. 89 (2014) 2827–2832.

[20] V.M. Starov, S.R. Kosvintsev, V.D. Sobolev, M.G. Velarde, S.A. Zhdanov, Spreading of Liquid Drops over Saturated Porous Layers, Coll. Interface Sci. 246 (2002) 372-379.

[21] G. Pucella, E. Alessi, L. Amicucci, B. Angelini, M.L. Apicella, G. Apruzzese et al., Overview of the FTU results, Nucl. Fusion 55 (2015) 104005 (11pp).